

EFFECT OF OXYGEN CARRIER PARTICLE SIZE ON THE HYDRODYNAMICS OF FUEL REACTOR IN A CHEMICAL LOOPING COMBUSTION SYSTEM

Mit Manojbhai Sheth, Atal Bihari Harichandan

Department of Mechanical Engineering,

Marwadi Education Foundation Group of Institution - Rajkot, (India)

ABSTRACT

The hydrodynamics of fuel reactor in a CLC system has been analyzed by using a multiphase CFD-based model with gas-solid interactions and chemical reactions. In this paper, the fuel reactors of two CLC systems are numerically simulated independently by using hydrogen with calcium sulfide as oxygen carrier, and methane with copper oxide as oxygen carrier in similar conditions. Kinetic theory of granular flow has been adopted. An Eulerian multiphase model is used to describe continuum two-fluid model for both gas and solid phases. Conservation of mass, momentum and species equations, and reaction kinetics of oxygen carriers are used for the numerical simulation. The bubble hydrodynamics in both the fuel reactors are analyzed. Numerical simulations are carried out to capture the bubble hydrodynamics and analyze the effect of different granular size oxygen carriers on the hydrodynamics of fuel reactor in a chemical looping combustion system.

Keywords: Bubble Hydrodynamics, Chemical Looping Combustion, Different Particle Sizes, Fuel Reactors, Kinetic Theory of Granular Flow

I. INTRODUCTION

The rising concentration of CO₂ in the atmosphere due to increased energy consumption from fossil fuels has been the real concern for many researchers. Chemical looping combustion (CLC) is a novel combustion technology with inherent separation of greenhouse CO₂. It is considered to be an environmentally superior method with a low energy penalty as compared to that of other carbon capture technologies like pre-combustion, oxy-fuel combustion or post-combustion due to the fact that the CO₂ from the combustion process is inherently not diluted with nitrogen which would otherwise require energy intensive processing [1]. It employs a dual fluidized bed system with metal oxide being employed as oxygen supplier for combustion in the fuel reactor. The reduced metal is then re-oxidized in the air reactor before being re-introduced back to the fuel reactor completing the loop. CLC system eliminates the formation of nitrogen oxide (NO_x) producing a flue gas composed primarily of carbon dioxide and water vapor. But, hydrogen fueled CLC produces only steam in the reduction reactor which can be expanded to very low pressure with high expansion which increases the efficiency of any power plant significantly.

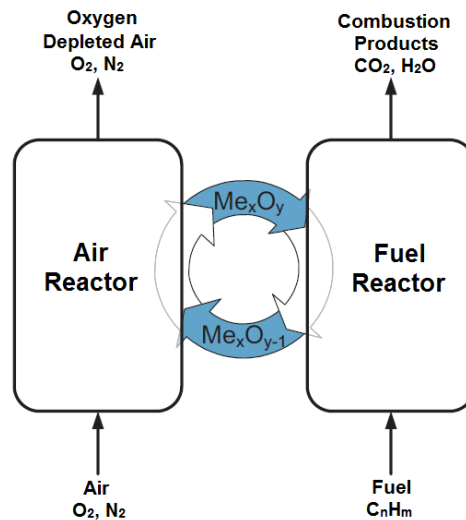
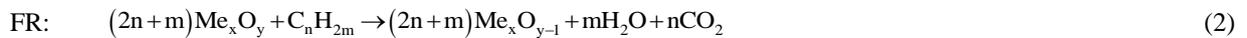


Fig. 1. Schematic view of CLC process.

Figure 1 represents the schematic view of a CLC system and illustrates its basic working principle. The reactions in both the reactors are expressed as:



Here, Me_xO_y represents a metal oxide. The oxidation of the particles in the air reactor is exothermic whereas the reduction reaction in the fuel reactor can be either exothermic or endothermic depending on the fuel and the oxygen carrier material used in the reactor.

Computational fluid dynamics (CFD) models based on the fluid dynamics and reaction kinetic mechanisms are used for better understanding of the complex gas flow and solids distribution in the reactors involved in a CLC system. The CFD models are based on the first principles of momentum, heat and mass transfer and do not require detailed assumptions in the modeling procedure like that of macroscopic fluid dynamics models. These models can simulate the behavior of the reactor during a transient time until the steady state is reached. The resistance to gas diffusion between bubbles and emulsion phases plays a major role in the dense bed of fluidized bed reactor. In recent past, many numerical and experimental studies has been performed on this novel technology [2-9] with solid, liquid and gas fuels and various oxygen carrier metals such as Fe, Ni, Mn, Cu, and Ca.

Due to rising concerns about global energy and environmental greenhouse problems, hydrogen is expected to be one of the most important energy carriers in next decades. Therefore, effective use of hydrogen energy and evaluating the novel scenarios of hydrogen implementation has drawn continuous interests amongst several researchers. The hydrogen fueled CLC process produces pure steam in the fuel reactor without any CO₂ emission. This steam from the reduction reactor can be expanded to very low pressure with high expansion when used in the gas turbine cycle of a power plant giving rise to production of much more power from the turbine. It has a breakthrough performance with at least about 12% higher efficiency compared to the gas turbine

cycle with conventional H_2/O_2 combustion and is environmentally superior due to complete elimination of NO_x formation [10]. The exergy losses in combustion and power consumption are much lower than those in the H_2/O_2 combined cycle [11].

With due consideration to the very limited numerical study on bubble hydrodynamics in fuel reactor of a CLC system, the aim of the work presented in this paper is: (i) to analyze the effects of fuel and oxygen carriers on the hydrodynamics of fuel reactor in a H_2 -fueled CLC system by using a multiphase CFD-based model and (ii) to compare the performance of the same model with methane-fueled CLC system in similar operating conditions. Figure 2 represents two interconnected fluidized bed reactors in which $CaSO_4$ (metal-oxide) is reduced by H_2 to calcium sulfide (CaS) in the fuel reactor and CaS is transported to air reactor to be oxidized back to $CaSO_4$. The same system can be used for methane fueled CLC system in which the metal oxide (CuO) is reduced by CH_4 to copper (Cu) in the fuel reactor and Cu is transported to air reactor to be oxidized back to CuO.

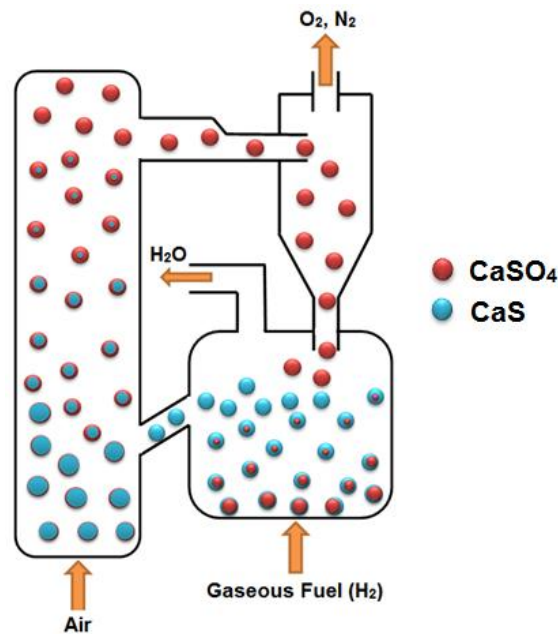


Fig. 2. CLC system with two interconnected fluidized bed reactors.

For the present work, the reactions occurring in the fuel reactors of these CLC systems are expressed as:



The reaction of Eq. (3) is exothermic reduction reaction of $CaSO_4$ and H_2 with low-level energy release in a low-temperature region ($\approx 600\text{-}1200\text{ K}$) and the reaction of Eq. (4) is an endothermic reduction reaction of CuO and CH_4 .

II. MATHEMATICAL MODELING

In contrast to the Eulerian-Lagrangian treatment used for the discrete phase model, an Eulerian multiphase treatment is used for each phase in the present approach. The continuity, momentum and energy equations are

solved for each phase whereas a single pressure is shared by all phases. The description of multiphase flow as interpenetrating continua incorporates the concept of phasic volume fractions (α_q).

The general hydrodynamic equations solved for transient and isothermal fluid-solids in each phase are given as follows:

2.1. Continuity equations:

The continuity equation for phase a is:

$$\frac{\partial}{\partial t}(\alpha_a \rho_a) + \nabla \cdot (\alpha_a \rho_a \vec{v}_a) = \sum_{b=1}^n (\dot{m}_{ba} - \dot{m}_{ab}) + S_a \tag{5}$$

where ρ_a and \vec{v}_a are the density and velocity of phase a respectively and \dot{m}_{ba} represents the mass transfer from the b^{th} to a^{th} phase, and \dot{m}_{ab} characterizes the mass transfer from phase a to phase b . S_a is the source term.

The mass, momentum and heat exchange among different gas and solid phases are involved while considering continuity equation in a heterogeneous reaction.

2.2. Momentum equations:

The momentum equation for phase a is:

$$\frac{\partial}{\partial t}(\alpha_a \rho_a \vec{v}_a) + \nabla \cdot (\alpha_a \rho_a \vec{v}_a \vec{v}_a) = -\alpha_a \nabla p + \nabla \cdot \bar{\bar{\tau}}_a + \alpha_a \rho_a \vec{g} + \sum_{b=1}^n (\bar{R}_{ba} + \dot{m}_{ba} \vec{v}_{ba} - \dot{m}_{ab} \vec{v}_{ab}) + (\vec{F}_a + \vec{F}_{lift,a} + \vec{F}_{vm,a}) \tag{6}$$

where $\bar{\bar{\tau}}_a$ is the a^{th} phase stress-strain tensor.

$$\bar{\bar{\tau}}_a = \alpha_a \mu_a (\nabla \vec{v}_a + \nabla \vec{v}_a^T) + \alpha_a \left(\lambda_a - \frac{2}{3} \mu_a \right) \nabla \cdot \vec{v}_a \vec{I} \tag{7}$$

Here μ_a and λ_a are the shear and bulk viscosity of phase a , \vec{F}_a is an external body force, $\vec{F}_{lift,a}$ is a lift force, $\vec{F}_{vm,a}$ is a virtual mass force, \bar{R}_{ba} is an interactive force between phases, and p is the pressure shared by all phases.

\vec{v}_{ba} is the interphase velocity. If mass transfer takes place from phase b to phase a (i.e., $\dot{m}_{ba} > 0$), $\vec{v}_{ba} = \vec{v}_a$; whereas for mass transfer from phase a to phase b (i.e., $\dot{m}_{ba} < 0$), $\vec{v}_{ba} = \vec{v}_b$. Similarly, if $\dot{m}_{ab} > 0$ then $\vec{v}_{ab} = \vec{v}_a$, if $\dot{m}_{ab} < 0$ then $\vec{v}_{ab} = \vec{v}_b$.

Friction, pressure, cohesion, and other effects collectively influence the value of \bar{R}_{ba} , and based on the physical conditions, $\bar{R}_{ba} = \bar{R}_{ab}$ and $\bar{R}_{aa} = 0$. The velocity gradients in the gaseous (primary) phase flow field in a multiphase flow generate lift forces ($\vec{F}_{lift,a}$) that act on solid particles. These forces are more substantial for bigger particles. In the present model, the particle diameter being much smaller than the inter-particle spacing, the inclusion of lift forces is insignificant and they are also negligible as compared to drag forces. So, these forces are not included in the calculation. The virtual mass force ($\vec{F}_{vm,a}$) is considered when a solid phase (secondary, b) accelerates relative to the gas phase (primary, a). The inertia of the primary-phase mass encountered by the accelerating particles (or bubbles or droplets) exerts a virtual mass force on the particles.

This force is significant when the secondary phase density is much smaller than the primary phase density and is, therefore, not included in the present calculation.

2.3. Species transport equations:

The conservation equations for chemical species in multiphase flows for each phase a predict the local mass fraction of each species, Y_i^a through the solution of a convection-diffusion equation for the i^{th} species. For multiphase flow, the generalized chemical species conservation equation can be presented in the following form:

$$\frac{\partial}{\partial t}(\rho^a \alpha^a Y_i^a) + \nabla \cdot (\rho^a \alpha^a \bar{v}^a Y_i^a) = -\nabla \cdot \alpha^a \bar{J}_i^a + \alpha^a R_i^a + \alpha^a S_i^a + \sum_{b=1}^n (\dot{m}_{b \rightarrow a}^i - \dot{m}_{a \rightarrow b}^i) + \mathfrak{R} \tag{8}$$

where R_i^a is the net rate of production of homogeneous species i by chemical reaction for phase a , $\dot{m}_{a \rightarrow b}^i$ is the mass transfer source between species i and j from phase a to b , and \mathfrak{R} is the heterogeneous reaction rate. In addition, α^a is the volume fraction for phase a and S_i^a is the rate of creation by addition from the dispersed phase and any user defined sources. \bar{J}_i^a is the diffusion flux of species i which arises due to gradients of concentration and temperature. The mass diffusion due to concentration gradients is modeled by using the dilute approximation (also called Fick's Law) as:

$$\bar{J}_i^a = -\left(\rho D_{i,m} + \frac{\mu_t}{Sc_t}\right) \nabla Y_i^a \tag{9}$$

where $D_{i,m}$ is diffusion coefficient of the mixture (m^2/s) and Sc_t is the turbulent Schmidt number ($\frac{\mu_t}{\rho D_i}$ where

μ_t is the turbulent viscosity and D_i is the turbulent diffusivity) and is chosen to be 0.7 for calculations.

2.4. Kinetic theory of granular flow:

A random granular motion of particles is likely to occur due to collision of solid particles inside the reactor. A transport equation for solid phase [12] can describe this random motion of particles as:

$$\frac{\partial}{\partial t}(\alpha_{sol} \rho_{sol} \Theta_{sol}) + \nabla \cdot (\alpha_{sol} \rho_{sol} \Theta_{sol} \mathbf{u}_{sol}) = -\frac{2}{3} \left(p_{sol} \bar{I} + \alpha_{sol} \bar{\bar{v}}_{sol} \right) : \nabla \bar{\mathbf{u}}_{sol} + \nabla \cdot (k_{sol} \nabla \Theta_{sol}) - \gamma - 3\beta_{gs} \Theta_{sol} \tag{10}$$

Here, Θ_{sol} is granular temperature and is given by: $\Theta_{sol} = \frac{1}{3} \langle u'_{sol} u'_{sol} \rangle$, where u'_{sol} is the fluctuating velocity of the particles and can be derived from $u'_{sol} = V_{sol} - u_{sol}$, and p_{sol} is solid pressure. β_{gs} is the interphase momentum transfer for calculating drag between solid phase and gas phase. If $\alpha_{gas} < 0.8$, the well-known Ergun equation [13] is suitable for describing the dense regime:

$$\beta_{gs} = 150 \frac{(1 - \alpha_{gas}) r_{sol} \mu_{gas}}{\alpha_{gas} d_{sol}^2} + 1.75 \frac{\rho_{gas} \alpha_{sol} |u_{gas} - u_{sol}|}{d_{sol}} \tag{11}$$

If $\alpha_{gas} > 0.8$, the drag coefficient is calculated by the equation proposed by Wen and Yu [14]:

$$\beta_{gs} = \frac{3}{4} C_d \frac{|u_{gas} - u_{sol}|}{d_{sol}} \alpha_{gas}^{-2.65} \tag{12}$$

$$C_d = \begin{cases} \frac{24}{Re} (1 + 0.15 Re^{0.687}), & Re \leq 1000 \\ 0.44, & Re > 1000 \end{cases} \quad (13)$$

$$\text{and } Re = \frac{|u_{gas} - u_{sol}| \alpha_{gas} \rho_{gas} d_{sol}}{\mu_{gas}} \quad (14)$$

2.5. Closure models:

The constitutive closure models in the present model in order to close the above mentioned governing equations are followed as below:

2.5.1. Interphase exchange coefficient

The solid-fluid interchange exchange coefficient ($K_{exchange}$) in its general form is expressed as:

$$K_{exchange} = \frac{\alpha_{sol} \rho_{sol} F}{t_{sol}} \quad (15)$$

where F is a factor that depends on drag function (C_D) and relative Reynolds number (Re_s) [15].

$$F = \frac{C_D Re_{sol} \alpha_{liq}}{24 v_{r,sol}^2} \quad (16)$$

$$\text{and } C_D = \left(0.63 + \frac{4.8}{\sqrt{Re_{sol} / v_{r,sol}}} \right)^2$$

The volume fraction and relative Reynolds number (Re_{sol}) of solid particles along with the terminal particle velocities influence the values of F and C_D .

$$Re_{sol} = \frac{\rho_{gas} d_{sol} |\vec{v}_{sol} - \vec{v}_{gas}|}{\mu_{gas}} \quad (17)$$

where the subscript gas is for the gas phase, sol is for the solid phase, and d_{sol} is the diameter of the solid phase particles.

$v_{r,sol}$ is the terminal velocity correlation for the solid phase and is given by:

$$v_{r,sol} = 0.5 \left(\frac{A - 0.06 Re_{sol}}{+\sqrt{(0.06 Re_{sol})^2 + 0.12 Re_{sol} (2B - A) + A^2}} \right) \quad (18)$$

$$A = \alpha_{gas}^{4.14} \quad (19)$$

$$\text{and } B = \begin{cases} 0.8 \alpha_{gas}^{1.28}, & \alpha_{gas} \leq 0.85 \\ \alpha_{gas}^{2.65}, & \alpha_{gas} > 0.85 \end{cases} \quad (20)$$

t_{sol} is the particulate relaxation time defined as:

$$t_{sol} = \frac{\rho_{sol} d_{sol}^2}{18\mu_{gas}} \quad (21)$$

where d_{sol} is the diameter of particles in solid phase.

2.5.2. Fluid-solids drag force

The motion of solid particles through a viscous fluid inside the fuel reactor often experiences a resistance due to interphase drag forces between solid-liquid phases. The solid-gas interactions are described by the interphase momentum exchange and the drag correlation based on the settling of beds and the terminal velocity of fluids [15] as:

$$F_{gs} = F_{sg} = \frac{3\mu_{gas}\alpha_{sol}\alpha_{gas}}{4v_{r,sol}d_{sol}^2} \left(0.63\sqrt{Re_s/v_{r,sol}} + 4.8 \right)^2 \quad (22)$$

2.5.3. Solids pressure

For the cases of granular flows where the solids volume fraction is less than its maximum allowed value (compressible regime), a solids pressure is calculated independently and used for the pressure gradient term in the granular-phase momentum equation. The solids pressure is composed of a kinetic term and a term due to particle collisions as:

$$P_{sol} = \alpha_{sol}\rho_{sol}\Theta_{sol} + 2\rho_{sol}(1+e_{resti})\alpha_{sol}^2g_{0,resti}\Theta_{sol} \quad (23)$$

where e_{resti} is the coefficient of restitution for particle collisions, $g_{0,resti}$ is the radial distribution function, and Θ_{sol} is the granular temperature that is proportionate to the kinetic energy of the fluctuating particle motion.

II. NUMERICAL CONSIDERATION

In the present model, a finite-volume method based on phase-coupled SIMPLE (PC-SIMPLE) algorithm [20] has been used to solve the non-linear coupled partial differential equations of multiphase flow problems with additional features of kinetic theory and reaction equations. The commercial CFD software code FLUENT was used for solving the coupled equations by adopting second order upwind differencing scheme. Time step of 0.0005 was chosen. A convergence criterion of 10^{-3} was considered for each scaled residual component. The velocities are solved in a segregated manner, but they are coupled by phases. The block algebraic multi-grid (AMG) scheme was also used by the density based solver to coarsen grids so that the numbers of iterations are reduced and the faster convergence of the solution is achieved. The numerical results being dependent on the quality and quantity of the finite volume cells, grid independence study has its importance. However, the present simulations were performed with 2500 rectangular cells in the computational domain. The present grid follows the thumb rule of grid independence test for simulation of circulating fluidized bed reactors reported by many researchers where the size of the elementary cell is 10 times of the particle diameter. Figure 3 shows the schematic and grids used for the fuel reactor.

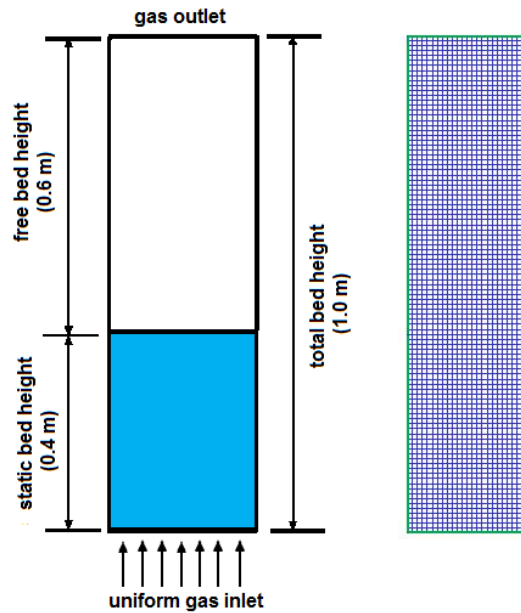


Fig. 3. Schematic and grid of the fuel reactor.

For the present simulation, Gunn's [13] heat transfer coefficient was used. The dispersed $k-\varepsilon$ turbulence model for the turbulent predictions of the continuous phase has been considered. The restitution coefficient between the solid particles was chosen as 0.9. Velocity inlet condition for the inlet and outflow condition for the outlet of the reactor were defined as the boundary conditions. No-slip condition was used for the gas-solid phase at the wall. The second order QUICK scheme was used for the evaluation of convective terms.

The bed was initially filled with particles up to 0.4 m high (static bed height). The total volume fraction of solids of 0.48 was patched in the static bed height. The maximum particle packing was assigned to $\varepsilon_{s,max} = 0.6$ so as to prevent the spacing between the particles from decreasing to zero. The computational domain of the reactor was discretized by 2500 rectangular cells. For reaction kinetic, the shrinking-core model for grain geometry has been applied which considers the oxygen carriers composed by a matrix of non-porous individual grains of uniform size. The present numerical work is based on the simulation model parameters used by Deng et al. [19]. However, for methane-fueled reactor, particle density and gas density are 6670 kg/m^3 and 0.6679 kg/m^3 respectively with all other parameters being same as the base case. Both the reactors are simulated for different temperatures between 750 K - 1250 K

IV. RESULTS

A multiphase computational fluid dynamics model based on kinetic theory of granular flow has been numerically simulated to describe the hydrodynamics and chemical reactions of dense gas-solid flows. CFD simulation is used for capturing the salient features of bubble formation, rise and burst. The simulations are carried out for different particle sizes of the granules.

A multiphase computational fluid dynamics model based on kinetic theory of granular flow has been numerically simulated to describe the hydrodynamics and chemical reactions of dense gas-solid flows. CFD

simulation is used for capturing the salient features of bubble formation, rise and burst. The simulations are carried out for different particle sizes of the granules. A relation between bubble formation and molar fraction of reactants and products in gas phase has been studied from the numerical results.

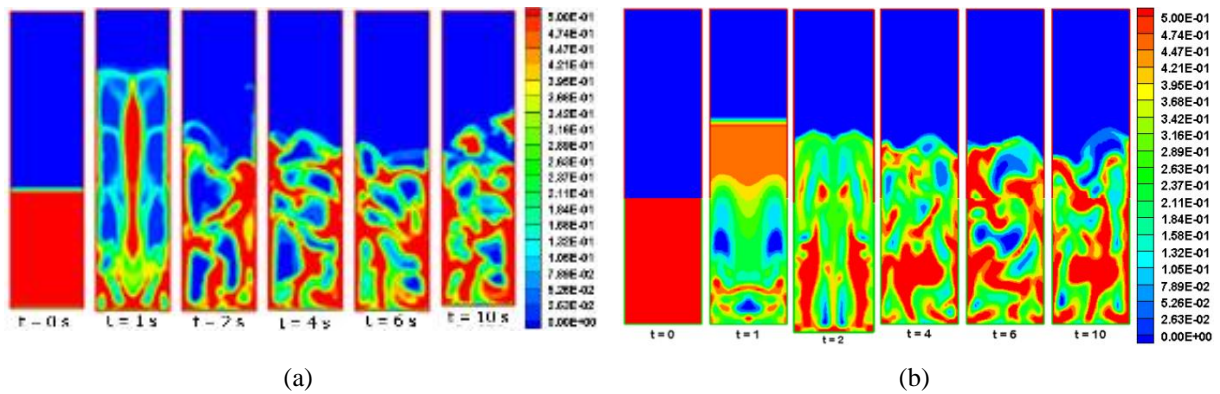


Fig. 4. Unsteady development of solid volume fraction contour with quasi steady reaction rate.

Figure 4 (a) and 4 (b) shows the unsteady bubble dynamics of solid volume fraction contour with quasi-steady reaction rate at different instantaneous time between 0 – 10 s for hydrogen and methane as a fuel and calcium sulphate and copper oxide as an oxygen carrier particles respectively. The gas velocity being relatively higher inside the bubbles and smaller in the slugs, bubbles move significantly faster as compared to the gas in the emulsion phase. Thus, the reaction rate is higher in the emulsion region where most of the solid particles are present and low in the bubble region where solid particles are almost absent. The transient behavior of bubble dynamics is observed within first 1.0 s of simulation after which quasi-steady reaction state is attained. The conversion rate is higher in the case when CH₄ as a fuel and CuO as metal oxide as shown in figure 4 (b).

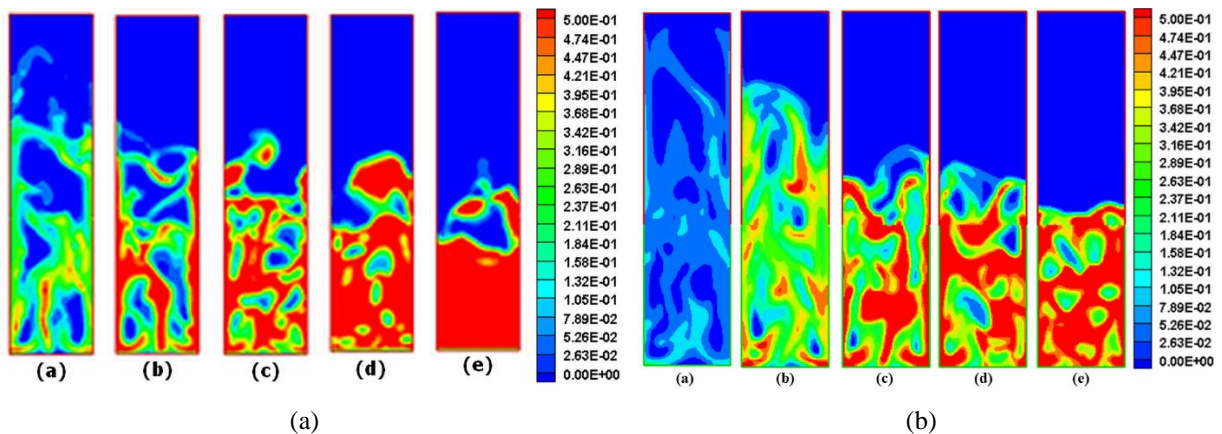


Fig. 5. Solid volume fraction contour with different particle sizes (a) $D_p = 100 \mu\text{m}$, (b) $D_p = 200 \mu\text{m}$, (c) $D_p = 275 \mu\text{m}$, (d) $D_p = 300 \mu\text{m}$ and (e) $D_p = 400 \mu\text{m}$.

Figure 5(a) and 5(b) shows the variation of solid volume fraction contour for different particle sizes like 100 μm , at instantaneous time of $t = 10.0 \text{ s}$ for hydrogen and methane as a fuel and calcium sulphate and copper oxide as an oxygen carrier particles respectively. For all the cases, the static bed height, free board height and the width of the reactor are kept fixed at 40 cm, 60 cm and 25 cm respectively. The global mixing of gas-solid particles has been found to be considerably superior for the reactors with smaller granule sizes. The velocity of gas and emulsion in these reactors are relatively higher than the reactors with bigger particles. Thus the gas and

emulsion tend to spread over large part of the reactor. However, the reactors with bigger particles, instead of having more oxygen carriers in the dense bed region, experience very low reaction rates due to improper mixing of gas-solid particles. It is very well understood from figure 5 that the conversion rate of feed fuel gas can further be increased by considering nano-size oxygen carrier particles.

V. CONCLUSION

The reactive fluid dynamic system of the fuel reactor is modeled by incorporating the kinetic of oxidized metal reduction into the FLUENT code. Similar to the modeling of riser in a circulating fluidized bed combustor, authors have modeled the fuel reactor of the CLC system with different particle sizes of the metal oxide like 100 μm , 200 μm , 275 μm , 300 μm , 400 μm in the present work. A low conversion rate of feed fuel gas has been obtained which may be due to combined effect of low bed temperature, bigger particle size, smaller dense bed height and larger bed width of the reactor. The velocity and gas emulsion are relatively higher in the reactors with smaller particles. The conversion rate is decrease with the particle sizes of granular particles increases. All these parameters lead to fast and large bubbles in the reactor which reduces the reaction rate and hence the conversion rate of the feed fuel gas. A significant increase in conversion rate can be obtained with smaller oxygen carrier particles (preferably of nano-size) which will enhance the overall performance of CLC plant as they do not generate large bubbles and proper mixing of gas-solid particles can very well be established.

REFERENCES

- [1] A.R. Bidwe, F. Mayer, C. Hawthorne, A. Charitos, A. Schuster and G. Scheffknecht, Use of ilmenite as an oxygen carrier in chemical looping combustion – Batch and continuous dual fluidized bed investigation. *Energy Procedia*, 4, 2011, 433-440.
- [2] H. Ritcher and K. Knoche, Reversibility of combustion processes. *ACS Symposium Series*, 235, 1983, 71-86.
- [3] H.J. Ryu, D.H. Bae, K.H. Han, S.Y. Lee, G.T. Jin and J.H. Choi, Oxidation and reduction characteristics of oxygen carrier particles and reaction kinetics by unreacted core model. *Korean J. Chem. Eng.*, 18, 2001, 831-837.
- [4] M. Ishida, M. Yamamoto and T. Ohba, Experimental results of chemical looping combustion with NiO/NiAl₂O₄ particle circulation at 1200 °C. *Energy Conv. Management*, 43, 2002, 1469-1478.
- [5] T. Mattison, M. Johansson and A. Lyngfelt, Multicycle reduction and oxidation of different types of iron oxide particles – application to chemical looping combustion. *Energy Fuels*, 18, 2004, 628-637.
- [6] A. Abad, T. Mattison, A. Lyngfelt and M. Ryden, Chemical looping combustion in a 300 W continuously operating reactor system using a manganese based oxygen carrier. *Fuel*, 85, 2006, 1174-1185.
- [7] H. Leion, T. Mattison and A. Lyngfelt, Solid fuels in chemical looping combustion. *Int. J. Greenhouse Gas Control*, 2, 2008, 169-179.



- [8] J. Jung and I.K. Gamwo, Multiphase CFD based models for chemical looping combustion process: Fuel reactor modeling. *Powder Technology*, 183, 2008, 401-409.
- [9] D. Berstad, R. Anantharaman and K. Jordal, Post-combustion CO₂ capture from a natural gas combined cycle by CaO/CaCO₃ looping. *Int. J. Greenhouse Gas Control*, 11, 2012, 25-33.
- [10] Z. Deng, R. Xiao, B. Jin and Q. Song, Numerical simulation of chemical looping combustion process with CaSO₄ oxygen carrier. *Int. J. of Greenhouse Gas Control*, 3, 2009, 368-375.
- [11] W. Shuai, Y. Yunchao, L. Huilin, W. Jiaying, X. Pengfei and L. Guodong, Hydrodynamic simulation of fuel-reactor in chemical looping process. *Chem. Eng. Research and Design*, 89, 2011, 1501-1510.
- [12] K. Mahalatkar, J. Kuhlman, E.D. Huckaby and T. O'Brien, Computational fluid dynamic simulation of chemical looping fuel reactors utilizing gaseous fuels. *Chem. Eng. Science*, 66, 2011, 469-479.